15

Development and study of magnetic shields for neutrino detector photomultiplier tubes under Neutrino-4M experiment on PIK and SM-3 reactors

© A.A. Mozhaiko,[1] S.A. Manninen,[1] L.V. Mukhamedzyanova,[1] P.A. Kuznetsov,[1] T.V. Knyazyuk,[1] A.P. Serebrov,[2] R.M. Samoilov,[2] V.V. Fedorov[2]

[1] National Research Center „Kurchatov Institute“ – Central Research Institute of Structural Materials „Prometei“, 191015 St. Petersburg, Russia
[2] National Research Center „Kurchatov Institute“ – Petersburg Nuclear Physics Institute, 188300 Gatchina, Leningrad Region, Russia
e-mail: npk3@crism.ru, annaanna-1996@mail.ru, serebrov_ap@pnpi.nrcki.ru

Received April 24, 2023
Revised August 4, 2023
Accepted August 27, 2023

A shielding system on the basis of MAP-1K rolled magnetic material was simulated and made, and is designed to protect photomultiplier tubes integrated in new neutrino detectors under NEUTRINE-4M experiment against Earth's magnetic field. Shielding coefficient was calculated for an individual cylindrical shield and assembly of 25 shields with the shielding structure axis directed along or across Earth's horizontal magnetic field. The obtained experimental data was compared with computer simulated data. Features of interaction between the shields in the system were examined. It was demonstrated that there is virtually no Earth's magnetic field effect on the detector performance when the detector is moved and rotated in the experiment with a new neutrino detector furnished with magnetic shields.

Key words: maximum permeability, amorphous soft magnetic alloys, magnetization distribution, magnetic shield, shielding coefficient , magnetization curve, neutrino detector, photomultiplier tube.

DOI: 10.61011/TP.2023.11.57510.104-23

Introduction

National Research Center „Kurchatov Institute“ — Petersburg Nuclear Physics Institute is working on a new neutrino detector for NEUTRINO-4M experiment for investigation of neutrino oscillations. NEUTRINO-4M experiment is carried out on SM-3 reactors (Rosatom) and is designed for PIK reactor (NRC„Kurchatov Institute“ — PNPI) [1–3]. Optical emission of the scintillator is recorded in this detector using two matrices consisting of 100 photomultiplier tubes (PEM). Each PEM is placed within a cylindrical protective enclosure. Even a weak Earth's magnetic field (EMF) degrades PEM performance. Magnetic shielding is one of EMF weakening methods [4–7]. Passive shielding using special soft magnetic materials is the simplest, cheapest, most reliable and sometimes the only possible method of weakening external magnetic fields. Amorphous soft magnetic cobalt-based alloys have already proved effective as a basic material for high-performance protective shields against permanent and alternating power frequency magnetic fields thanks to higher magnetic properties compared with crystalline equivalents and to the technological advantages: flexibility and wide shaping capabilities without losing magnetic properties [8,9]. In addition, amorphous alloys, compared with crystalline alloys, do not require expensive high temperature vacuum heat treatment, thus, reducing the shield manufacturing cost considerably.

„Neutrino-4“ experiment for the search for sterile neutrinos has detected an oscillation effect at the confidence level of three standard deviations [10]. To check the assumption that the effect is associated with the magnetic field effect on the PEM amplification coefficient, a task of PEM shielding against magnetic field is set. To improve considerably the experiment accuracy, the second neutrino laboratory is being made on SM-3 reactor (Dimitrovgrad, Russia) and a new neutrino detector is being developed. The scintillation type detector consists of four modules having a multi-sectional structure with 100 vertically arranged sections with PEM arranged on both sides of the section. It is shown that the experiment accuracy may be 2.7 times higher to achieve the confidence level more than 5 standard deviations and to answer the question whether sterile neutrinos exist, if the systematic effect is not confirmed. The new experiment is described in detail in a recent publication [3].

Control of possible systematic errors is one of the most important experiment tasks. This is why a special focus is made on PEM magnetic shielding, therefore it is required to protect PEM against EMF to check the assumption that the oscillation effect is associated with the magnetic field effect on the PEM amplification factor. Moreover, due the increase in statistical accuracy of the new system, the effect will be checked at a new accuracy level. The detector is mobile to

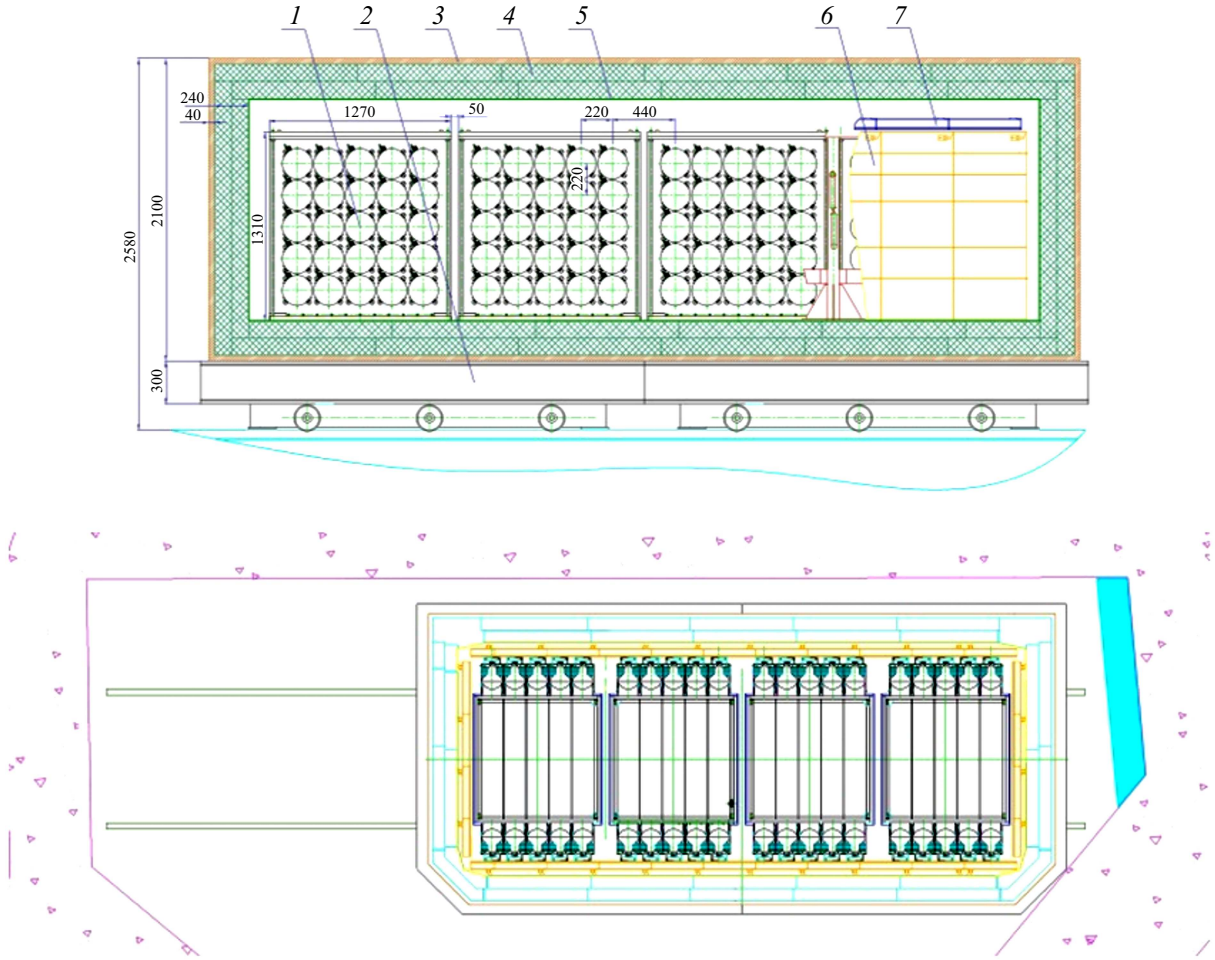

Figure 1. General arrangement of the reactor antineutrino detector mounted on a mobile platform (top) and layout of the detector in room 170 (bottom). *1* — antineutrino detector, *2* — mobile platform, *3* — copper, *4* — boronated polyethilene, *5* — boronated rubber, *6* — vertical active protection plates, *7* — top active protection plates.

provide the measurement of antineutrino flux dependence on the distance from the center of the reactor (Figure 1).

Magnetic field in this room depends not only on EMF, but also on the presence of support steel beams and lifting and handling equipment. Therefore, the magnetic field is inhomogeneous and each PEM must be shielded. Thus, section 10.2 in [11] reports that the magnetic field affects Hamamatsu PEMs and they must be shielded, whereby, to smooth edge effects, PEM shall be placed inside the shield in such a way that the distance between the PEM edge and shield edge is about one radius of the photocathode (Figure 12 in [11]). A magnetic shield for Hamamatsu R7081-100 PEM that fully encloses the photocathode is shown in [12]. The design of Neutrino-4M detector requires as close packing of PEM as possible, but backlighting between the sections shall be avoided, therefore diaphragms on the light waveguide ends within the liquid scintillator and diaphragms in front of the PEM light waveguide were used. The optimum geometry of light waveguides, diaphragm positions and PEM positions were defined by the computer simulation method. Such optimization is required to achieve the best detector resolution [3]. Compromise between backlighting and light collection defines the diaphragm positions and size of the cylindrical light waveguide in front of PEM (Figure 2). As a result, the center point of the cylindric hemispherical photocathode of PEM is 40 mm from the external magnetic shield cut. When the shield diameter is 210 mm, the magnetic field shielding effect at a distance of 40 mm axially is not sufficiently high compared with that in the shield center. As will be shown below, when this distance increases up to 65 mm, the shielding effect may be increased by 2 to 3 times. Therefore, the internal light waveguide that goes through the common housing of the neutrino detector and abuts against the scintillator reservoir glass was used to extend the shielding area by 25 mm. For this, it was covered with amorphous alloy tape on the outside and with reflecting mirror foil on the inside.

External aluminium cylinder (⌀211 mm) is attached to the wall (22 mm in thickness) of the multi-sectional neutrino detector that contains 25 such assemblies, and is covered

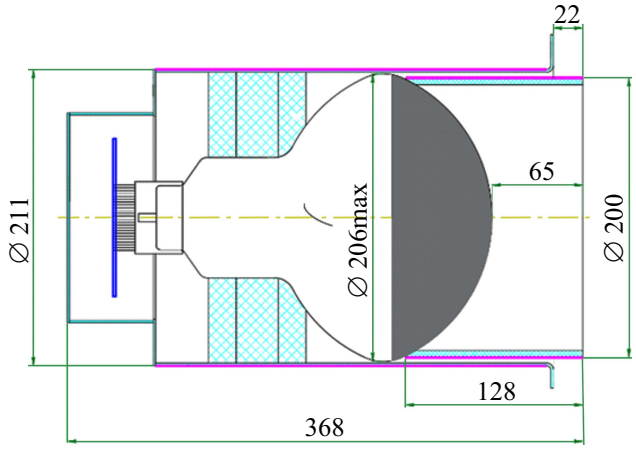

Figure 2. PEM and magnetic shield assembly.

with amorphous soft magnetic alloy tape to ensure PEM sheilding. The internal cylinder (⌀200 mm) is a light waveguide (covered with reflective mirror foil on the inside) that abuts against PEM on one side and against the plexiglass reservoir wall (30 mm), that is common for all 25 square light waveguides, on the other side (Figure 1). The internal cylinder (⌀200 mm) is covered with amorphous soft magnetic alloy tape to increase the PEM shielding area additionally by 25 mm.

Personnel of NRC „Kurchatov Institute"–„Central Research Institute of Structural Materials „Prometei" offer to shield PEMagainst Earth's magnetic field using MAR-1K rolled magnetic material designed on the basis of the amorphous alloy [13]. For this, shielding structures shall be made from MAR-1K material and their magnetic properties shall be investigated — that constitutes the objectives of this study. To ensure efficient shielding, dependence of the shielding coefficient (SF) on the number of layers of MAR-1K rolled magnetic material MAP-1K is investigated. It should be noted that the investigation of SF of the structures to be designed is a complex task for solution of which both design and experimental methods were used [14].

1. Materials and research methods

MAR-1K rolled material was made from Co-Fe-Ni-Cr-Mn-Si-B amorphous magnetic alloy tapes 30 mm in width and 20 μm in thickness, exposed to heat treatment by a method developed by NRC „Kurchatov Institute"–Central Research Institute of Structural Materials „Prometei". Magnetic properties of the alloy were measured according to the procedure described in GOST 8.377-80 on toroidal samples using MK-3E magnetometer system to record the main magnetization cure and permeability. Figure 3 shows a magnetization curve (B-H curve) for the given alloy after heat treatment. Initial relative permeability of the alloy was equal to 12 000, and maximum relative permeability was equal to 800 000. The measured magnetization curve was used to set magnetic properties of the shielding material during numerical calculation of SC.

MAR-1K rolled magnetic material was mounted on the cylindrical protective enclosure (Figure 4) of PEM with an outside radius of $R = 106$ mm and a length of $H = 265$ mm.

Magnetic induction was measured in natural Earth's magnetic field. The absolute value of magnetic induction vector inside the shielding structure was measured using MT-4 three-component fluxgate magnetometer. This magnetometer uses the differential magnetic induction measurement method based on magnetic induction compensation within the sensor's magnetic core. Magnetic induction measurement error by components is equal to 40 nT, magnetic induction absolute value measurement error is equal to 50 nT.

To find SC, absolute value of magnetic field induction was measured in the measurement region without shield and inside the shield ($B_{(\text{without screen})}$ and $B_{(\text{inside the screen})}$). SC was calculated using the following equation:

$$SC = B_{(\text{without screen})}/B_{(\text{inside the screen})}.$$

SC was also determined by calculation to obtain the magnetic field distribution within the whole shielding system volume and to review various positioning options relative to

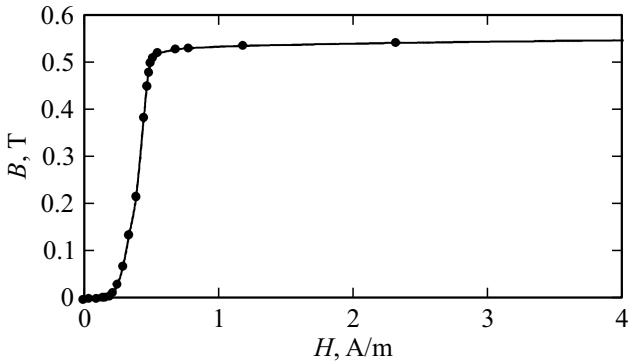

Figure 3. magnetization curve

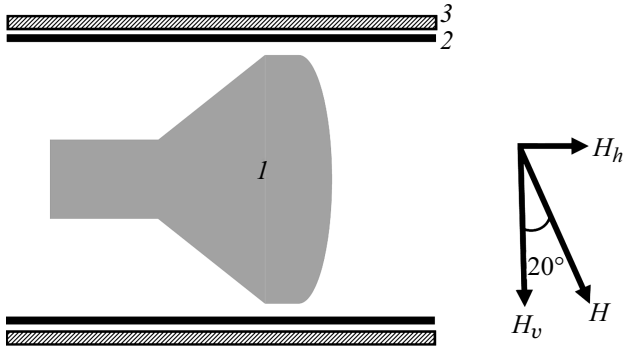

Figure 4. PEM shielding system layout. *1* — PEM, *2* — enclosure, *3* — MAR-1K rolled magnetic material, H — EMF, whereH_h is the horizontal component, H_v is the vertical component of EMF.

EMF. EMF shielding was simulated by the finite element method [15,16] in COMSOL Multiphysics, including the „Magnetic field" module. The software solves the Maxwell's magnetic field equations using the scalar magnetic potential as a dependent variable. Non-linear magnetic properties of the material used in the shield are set using the magnesium curve (Figure 3) recorded experimentally on MK-3E magnetometer system. Magnetic shield as a thin high-permeability medium layer is described by a boundary condition of normal discontinuity of magnetic flux density and tangential magnetic field in the layer. The model implemented the choice of the number of MAR-1K layers.

For the calculation, EMF is directed at 20° to the vertical axis (Figure 4). This angle was defined according to geographical position of the laboratories where the investigations were carried out. The shielding system was placed horizontally and two cases of positioning with respect to EMF were addressed: the system axis is placed along or across the EMF horizontal component. The calculation was carried out for a single shield and an assembly of 25 shields, because PEM were placed in the assemblies of 25 shielding enclosures according to the design. When the shields are placed at a distance comparable with their diameter, they shall affect the shielding performance of each other.

2. Results and discussion

For the proposed cylindrical system, dependence of the magnetic field strength along the cylinder axis was calculated for various numbers of shielding layers (Figure 5). The calculation shows that for two MAR-1K layers, the magnetic field strength in the center of the shield is equal to 0.8 A/m, and for 20 layers the magnetic field strength decreases to 0.6 A/m. Thus, when the number of layers is from 2 to 20, the magnetic field strength is 1.4 times lower in the center of the shield and remains almost unchanged at the shield edges. Therefore, SC increase at the cylinder edge (photocathode center point position) cannot be achieved by increasing the number of shielding layers.

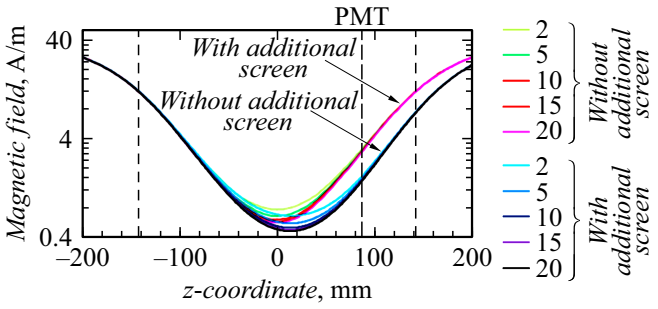

Figure 5. Magnetic field strength distribution along the cylinder axis for various numbers of MAR-1K layers (the cylinder axis is along the EMF horizontal component). $Z = 0$ corresponds to the center of the main shield. Two righthand and lefthand dashed lines mark the main shield ends. The vertical mark with PEM label shows the center point position of the photocathode.

The magnetic field along the cylinder axis as less dangerous, because the electrons flying primarily along the cylinder axis are not diverted by the magnetic field. Since the PEM sensitivity is higher in the EMF component perpendicular to the PEM axis, shielding is more relevant for the case when the PEM axis is placed across the EMF horizontal component.

It is better to place PEM at the enclosure edge to ensure the maximum photon receipt region, however, as shown in Figure 5, the magnetic field at the shield ends is shielded much worse than in the center of the system. In order to improve the shielding performance, a new system version with additional shield with a smaller inside radius of $R = 100$ mm and a length of $H = 128$ mm (Figure 2) is offered. The reduced diameter of the additional shield allowed to extent the shield up to the liquid scintillator reservoir glass wall. Whereby the center point of the PEM hemispherical photocathode, that has the worst position compared with other photocathode components that are placed closer to the shield center, is at a distance of 65 mm from the internal cylinder edge (marked with the dashed line in Figure 5). This point is considered to be the most critical, because SC increases considerably towards the center. Therefore, for further calculations and measurements, a control point was chosen — on the cylinder axis, 65 mm from the internal shield edge, at the location of the central section of the hemispherical photocathode.

Magnetic field was calculated for the new double shield system and the curves of strength distribution along the cylinder axis were drawn for various numbers of MAR-1K layers (Figure 5). The addition shield allowed the magnetic field to be reduced by a factor of 2.2 in the photocathode region compared with the first system version.

SC calculation with the shielding system axis placed in transverse and longitudinal directions with respect to the EMF horizontal component has shown that when the number of MAR-1K layers increases from 5 to 10, SC increases by 0.5% for longitudinal directions and by 3% for transverse direction (Figure 6, *a*). therefore, using more than 5 layers will be not feasible in terms of materials cost. The performed calculations suggested that two MAR-1K layers on the main and additional shields provide sufficient shielding at minimum cost. For the number of MAR-1K layers from 1 to 5 SC was measured experimentally, the measurements are shown in Figure 6, *b*. The experimental studies have shown that beginning from three MAR-1K layers, SC achieves approximately a constant level taking into account the measurement error and is equal to 5.5±0.5 for longitudinal direction of the EMF horizontal component and to 20±6 or the transverse direction. It should be noted that transverse field shielding is more important and the shielding coefficient equal to 10 is already sufficient.

Magnetic field strength distribution (H) in the plane 65 mm from the internal shield edge for three MAR-1K layers when the system axis is oriented transversely and longitudinally to the EMF horizontal component has shown

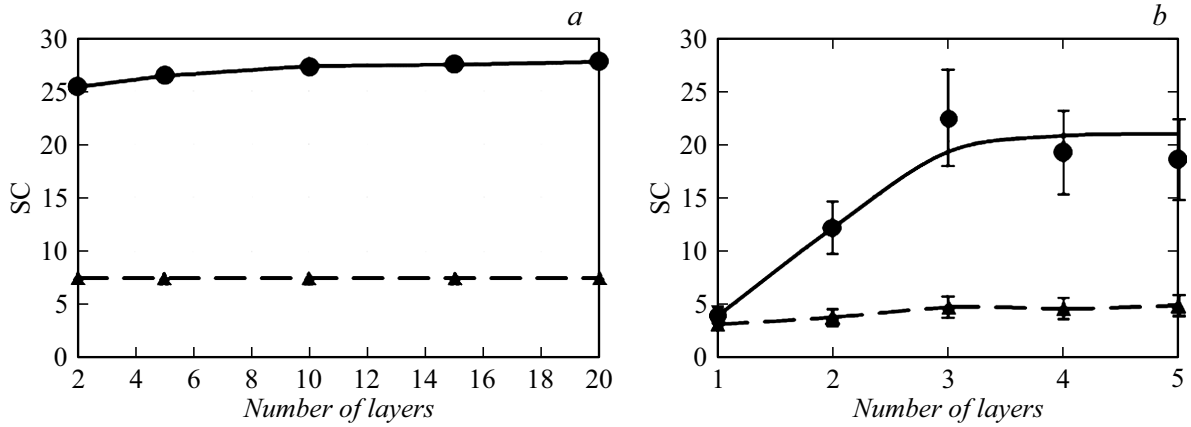

Figure 6. The design dependence (a) and experiment dependence (b) of SC on the number of MAR-1K layers in the test point (system axis is along (triangle) and across (circle) the EMF horizontal component).

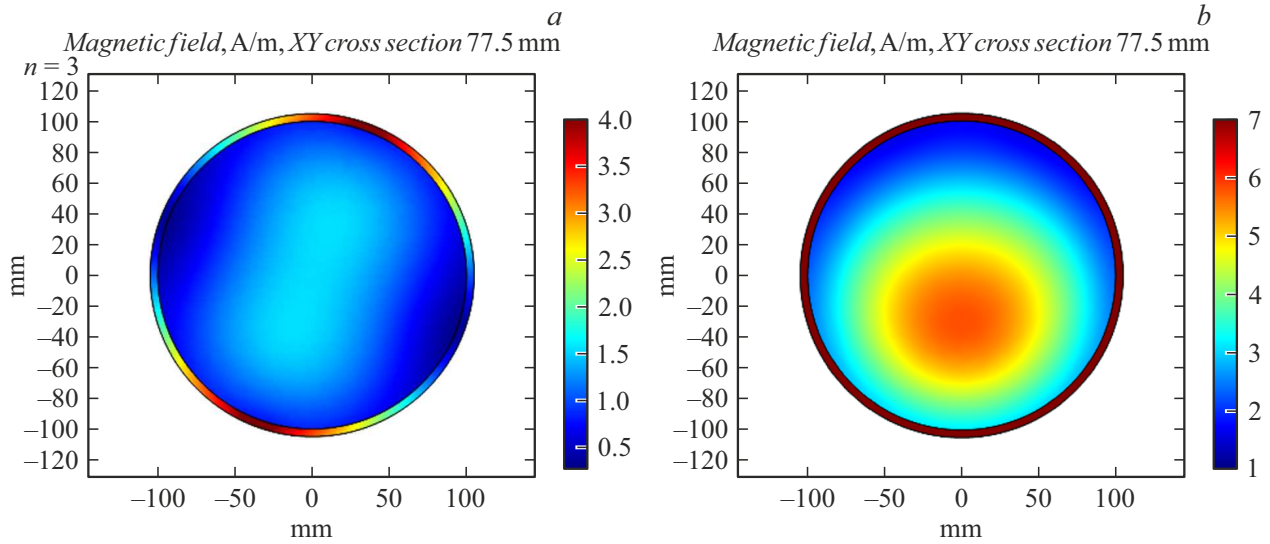

Figure 7. Magnetic field strength distribution H for three MAR-1K layers in the plane 65 mm from the edge of the internal cylindrical shield (the system axis is across (a) and along (b) the EMF horizontal component).

that for transverse orientation the strength inside the shield is axially symmetric about the EMF orientation (Figure 7, a). For parallel orientation, the maximum strength is observed on the bottom inside the shield, i.e. asymmetrically about the center due to the shielding system orientation with respect to EMF (Figure 7, b). However, it should be noted again that the longitudinal magnetic field is less dangerous.

Investigations of the magnetic field strength distribution in the shield oriented transversely and longitudinally with respect to the EMF horizontal component have shown that higher shielding performance is achieved by transverse orientation.

Magnetic field strength distribution (H) for the assembly of 25 cylinders shown in Figure 8 has shown that for the assembly orientation across the EMF horizontal component — the minimum magnetic field is observed in the center of the assembly and the maximum magnetic field is observed at the edges in shields 5 and 21 (Figure 8, b). For the assembly orientation along the EMF horizontal component, the interaction of the shields results in the maximum strength occurring in shields 21–25 on the bottom of the assembly. This is caused by the magnetic shield orientation and distortion of force lines within the assembly boundaries. Figure 8, d shows color marking of strength distribution in the side cross-section in the center of shields 3, 8, 13, 18, 23, and arrows indicate the magnetic field force line directions. At the shield edges where the force lines are concentrated, EMF enters the cylindrical shield to a longer distance. The magnetic field distribution pattern at the shield edges is also asymmetric, since EMF is oriented at 20° (Figure 8, c).

When comparing Figures 7, a and 8, b, 7, b and 8, c, it could be seen that the strength distribution behavior is similar in a single shield and in the assembly. For the

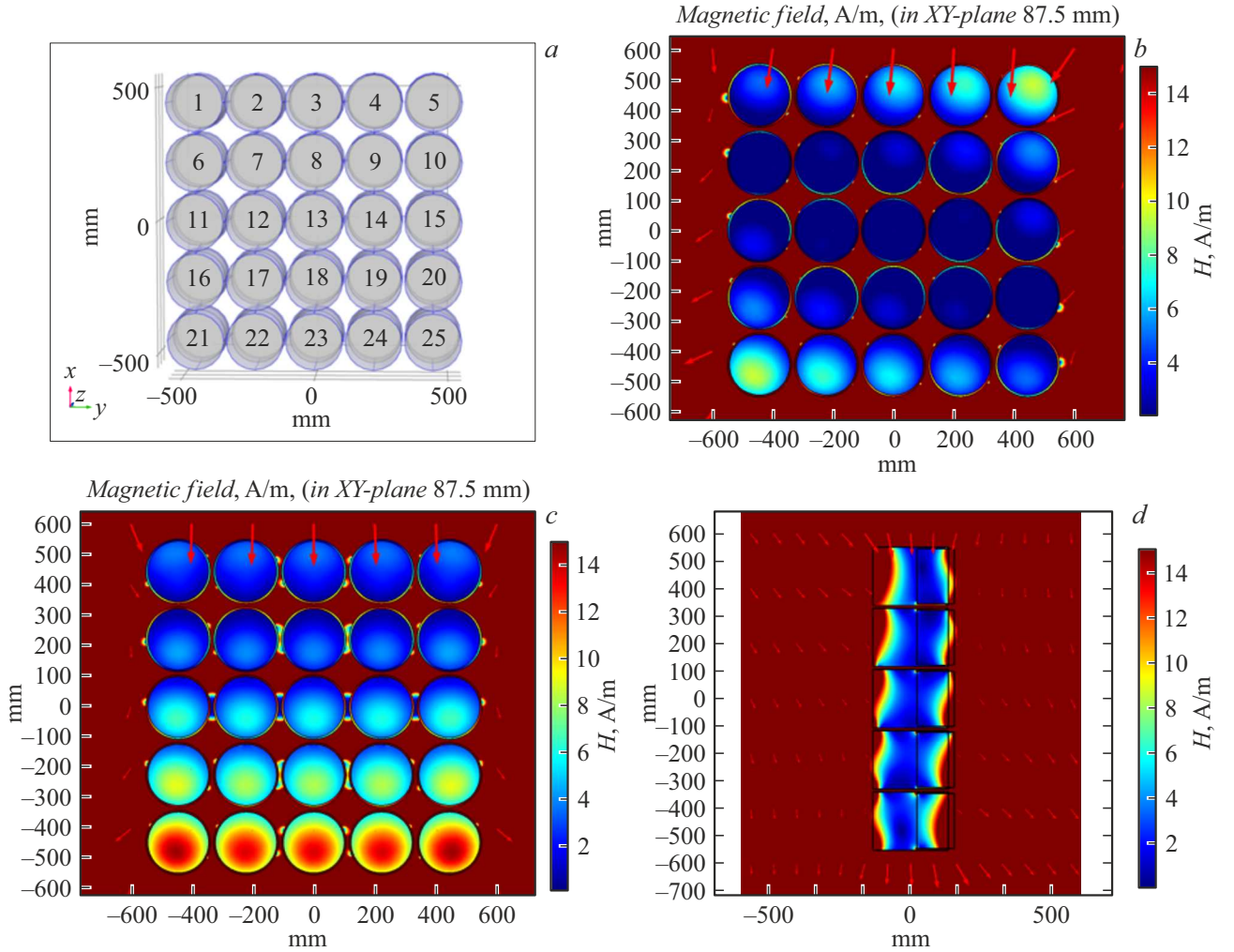

Figure 8. *a* — arrangement and numbering of magnetic shields in the assembly; *b* — magnetic field distribution in transverse section going through the control point (when the shield is placed across the EMF horizontal component); *c* and *d* — magnetic field strength distribution in transverse section (*c*) and longitudinal section (*d*) going through the control point (when the shield is placed along the EMF horizontal component).

assembly orientation across the EMF horizontal component, the lowest shielding performance is observed in the side components in the field direction. For the orientation along the EMF horizontal axis, the lowest shielding performance is observed on the bottom of the assembly. However, even in this case, the magnetic field has allowable values of 12 A/m due to the longitudinal magnetic field component.

For experimental investigations of the effect of the adjacent shields on each other, a mockup consisting of 25 shielded enclosures with three MAR-1K magnetic material layers was made (Figure 9). Magnetic induction was measured for each shield.

Figure 10 shows the experimental measurements of SC and their comparison with the simulation data. For system axis orientation across the EMF horizontal component, SC decreases at the assembly corners for shields 5 and 21. For system axis orientation along the EMF horizontal component, SC decreases in the lower row of the assembly.

The investigations have shown that the PEM shielding performance is higher when the system is oriented transversely to the EMF horizontal component. The detected features of the shield interaction in the assembly are in good agreement with the computer simulation data, therefore, this model may be used for calculation of similar systems.

The magnetic shield performance was examined using ET-Enterprises 9354KB scintillation detector with PEM amplitude analyzer (linearly focused dynode system) in vertical and horizontal orientations, scintillation source — Na-22 gamma radiation in NaI(Tl) crystal. The system setups are shown in Figure 11.

To check the dependence of the detector response on the PEM position in EMF, the horizontally oriented detector was rotated with intervals 45° about the vertical axis (Figure 11, *a*), and PEM was rotated about the axis horizontally (Figure 11, *b*) and vertically (Figure 11, *c*), energy peak positions of the source on the amplitude

Figure 9. Mockup of the assembly of 25 shields for the neutrino spectrum scintillation detector of NRC „Kurchatov Institute“ – PNPI.

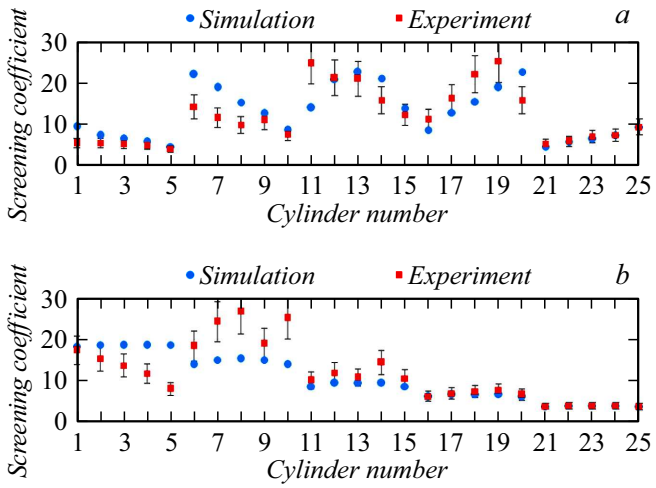

Figure 10. Comparison of SC calculation for each shield of the assembly of 25 shields for simulation and experiment purposes: the system axis is oriented transversely (a), and longitudinally (b) to the EMF horizontal component.

scale and relative variation of the position compared with the marked orientation were defined for each position. Spectra of the source in 8 PEM positions for rotation of non-shielded PEM (Figure 12, a) and shielded PEM (Figure 12, b) oriented vertically about the axis are shown in Figure 12. The average relative variation of energy peak positions in rotation for non-shielded and shielded PEM was

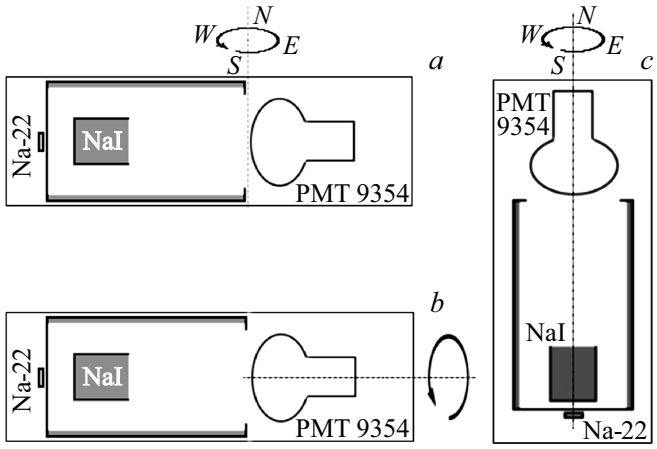

Figure 11. scintillation detector arrangement.

equal to 15% and less than 1%, respectively, in horizontal orientation for detector rotation about the vertical axis, 6% and less than 1% in horizontal orientation for PEM rotation about itself, 5% and less than 1% in vertical orientation for PEM rotation about itself.

Conclusion

Dependence of a single shield SC on the number of MAR-1K layers was established. Calculations and experimental investigations show that three MAP-1K magnetic material layers ensure maximum SC at minimum system fabrication cost.

Magnetic properties of a single shield and assembly of 25 shields made of MAR-1K magnetic material were investigated by calculation and experimental methods. Investigations of SC in the assembly of 25 frames shielded with MAR-1K rolled three-layer magnetic material have shown that SC decreases in corner shields in field direction for the system axis orientation across the EMF horizontal component, and in the lower row of the assembly for the system axis orientation along the EMF horizontal component. PEM shielding performance is maximum when the system axis is oriented transversely to the EMF horizontal component. However, PEM position and orientation in real conditions are defined by the scintillation detector specificetions.

EMF SC measured at a distance of 65 mm from the edge of the small shield is equal to at least 4.5 (with shield axis orientation along the EMF horizontal component) and at least 10 (with shield axis orientation across the EMF horizontal component) for all shields.

Dependence of the response of the detector with PEM shield with the given shield on the PEM position with respect to EMF was checked, relative response variation is lower than 1%.

Thus, the developed shielding system ensured the required protection of the new scintillation neutrino detector

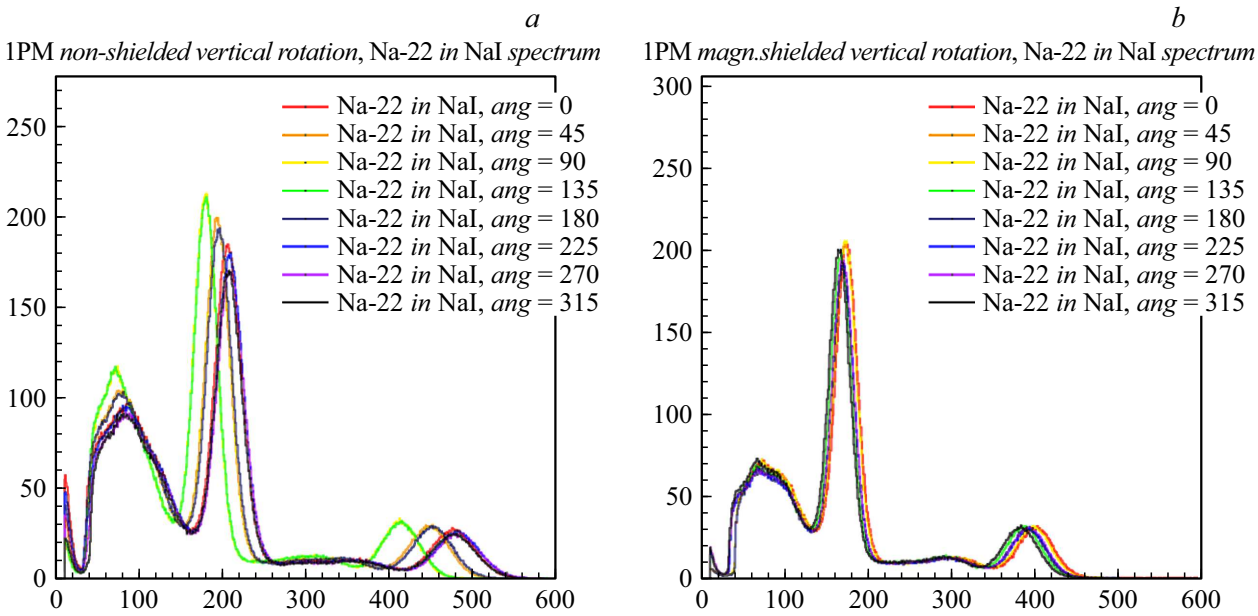

Figure 12. Spectra Na-22 in the detector with non-shielded PEM (*a*) and shielded PEM (*b*) rotated vertically.

PEM and may be recommended for application in such type of systems.

Conflict of interest

The authors declare that they have no conflict of interest.

References

[1] M.V. Kovalchuk, V.V. Voronin, S.V. Grigoriev, A.P. Serebrov. Crystallography Reports, **66** (2), 195 (2021). DOI: 10.1134/S1063774521020061

[2] M.V. Kovalchuk, S.L. Smolsky, K.A. Konoplev. Crystallografiya, **66** (2), 184 (2021)(in Russian). DOI: 10.31857/S0023476121020053

[3] A.P. Serebrov, V.G. Ivochkin, R.M. Samoilov, A.K. Fomin, V.G. Zinoviev, S.S. Volkov, V.L. Golovtsov, N.V. Gruzinskii, P.V. Neustroev, V.V. Fedorov, I.V. Parshin, A.A. Gerasimov, M.E. Zaytsev, M.E. Chaikovskii, A.M. Gagarskiy, A.L. Petelin, A.L. Izhutov, M.O. Gromov, S.A. Sazontov, A.A. Tuzov, V.I. Ryikalin, D.A. Makarenkov, A.M. Nemeryuk, T.E. Kuzmina. Tech. Phys., **93** (1), 166 (2023). DOI: 10.21883/TP.2023.01.55452.241-22]

[4] G. Ranucci, D. Giugni, I. Manno, A. Preda, P. Ullucci, A. Golubchikov, O. Smirnov. Nucl. Instrum. Methods in Phys. Res., **337**, 211 (1993). DOI: 10.1016/0168-9002(93)91156-H

[5] E. Calvo, M. Cerrada, C. Fernandez-Bedoya, I. Gil-Botella, C. Palomares, I. Rodrıguez, F. Toral, A. Verdugo. Nucl. Instrum. Methods in Phys. Res., **621**, 222 (2010). DOI: 10.1016/j.nima.2010.06.009

[6] M. Chen, B. Gao, J. Gao, H. He, C. Liu, H. Li, K. Li, L. Ren, S. Si, J. Wu, W. Wang, X. You. Nucl. Instrum. Methods in Phys. Res., **1039**, 167128 (2022). DOI: 10.1016/j.nima.2022.167128

[7] O. Smirnov, D. Korablev, A. Sotnikov, A. Stahl, J. Steinmann, V. Khudyakov, I. Avetissov, M. Zykova. JINST, **18**, P04015 (2023). DOI: 10.1088/1748-0221/18/04/P04015

[8] P.A. Kuznetsov, S.A. Manninen, O.V. Vasivieva. Voprosy materialovedeniya, **4** (68), 67 (2011).(in Russian)

[9] B.V. Farmakovsky, P.A.. Kuznetsov. V sb: *V Mezhdunarodny simpozium po elektromagnitnoi sovmestimosti i electromagnitnou ekologii EMS-2003, 16–19 sentyabrya 2003 g.*, sb. nauch. dokl. (SPbGETU „LETI“, SPb, 2003), s. 92–94. (in Russian)

[10] A.P. Serebrov, R.M. Samoilov, V.G. Ivochkin, A.K. Fomin, V.G. Zinoviev, P.V. Neustroev, V.L. Golovtsov, S.S. Volkov, A.V. Chernyj, O.M. Zherebtsov, M.E. Chaikovskii, A.L. Petelin, A.L. Izhutov, A.A. Tuzov, S.A. Sazontov, M.O. Gromov, V.V. Afanasiev, M.E. Zaytsev, A.A. Gerasimov, V.V. Fedorov. Phys. Rev. D, **104**, 032003 (2021). DOI: 10.1103/PhysRevD.104.032003

[11] Hamamatsu Photonics K.K. Photomultiplier Tubes and Assemblies for Scintillation Counting & High Energy Physics, TPMZ0003E01 APR. 2017 IP (2000) https://www.hamamatsu.com/content/dam/hamamatsu-photonics/sites/documents/99_SALES_LIBRARY/etd/High_energy_PMT_TPMZ0003E.pdf

[12] A.D. Avrorin, A.V. Avrorin, V.M. Aynutdinov, R. Bannash, I.A. Belolaptikov, D.Yu. Bogorodsky, V.B. Brudanin, N.M. Budnev, I.A. Danilchenko, G.V. Domogatsky, A.A. Doroshenko, A.N. Dyachok, Zh.-A.M. Dzhilkibaev, S.V. Fialkovsky, A.R. Gafarov, O.N. Gaponenko, K.V. Golubkov, T.I. Gress, Z. Honz, K.G. Kebkal, O.G. Kebkal, K.V. Konischev, A.V. Korobchenko, A.P. Koshechkin, F.K. Koshel, A.V. Kozhin, V.F. Kulepov, D.A. Kuleshov, V.I. Ljashuk, M.B. Milenin, R.A. Mirgazov, E.R. Osipova, A.I. Panfilov, L.V. Pan'kov, E.N. Pliskovsky, M.I. Rozanov, E.V. Rjabov, B.A. Shaybonov, A.A. Sheifler, M.D. Shelepov, A.V. Skurihin, A.A. Smagina, O.V. Suvorova, V.A. Tabolenko, B.A. Tarashansky, S.A. Yakovlev, A.V. Zagorodnikov, V.L. Zurbanov. EPJ Web Conf., **116**, 01003 (2016). DOI: 10.1051/epjconf/201611601003

[13] O.V. Vasilieva, A.S. Zhukov, P.A. Kuznetsov, A.K. Mazaeva, S.A. Minninen, T.V. Peskov, B.V. Farmakovsky. *Sposob polucheniya magnitnogo i elektromagnitnogo ekrana* (Pat. na izobretenie RU2636269 S1, 21.11.2017. Zayavka №2016144967 ot 16.11.2016)
[14] V.E. Mitrokhin, A.V. Ryapolov, A.E. Izvetiya Transsiba, **1** (17), 72 (2014).(in Russian)
[15] S.A. Manninen, P.A. Kuznetsov. Izmeritelnaya tekhnika, **6**, 8 (52) (in Russian).
[16] P.A. Kuznetsov, S.A. Manninen, A.A. Zhumagalieva. Izmeritelnaya tekhnika, **6**, 6 (52) (in Russian).

Translated by Ego Translating